# Laser-assisted deuterium-tritium fusion: A quantum dynamical model

N. Thomson, L. Moschini, and A. Diaz-Torres
*Department of Physics, Faculty of Engineering and Physical Sciences, University of Surrey, Guildford, Surrey GU2 7XH, United Kingdom*

(Received 27 March 2024; revised 17 July 2024; accepted 6 September 2024; published 19 September 2024)

Deuterium-tritium (D-T) fusion is a key to generating safe, clean, and limitless energy on Earth in future fusion power plants. Its understanding at low collision energies is incomplete, as D-T fusion is a quantum tunneling process affected by resonances whose origin is linked to properties of not fully understood nuclear forces. Simplified quantum dynamical calculations of laser-assisted D-T fusion are presented, suggesting that laser-nucleus interaction can enhance the average D-T fusion probability by 7–70% at deep subbarrier energies using laser fields of intensity $10^{27}$–$10^{29}$ W cm$^{-2}$ and a photon energy of 1 eV.

DOI: 10.1103/PhysRevC.110.034614

## I. INTRODUCTION

Nuclear fusion is an exciting next step in green energy production, boasting less nuclear waste than fission reactors while producing vastly more energy. The most promising nuclear process for generating such a sustainable energy future is the D-T fusion reaction [1,2], where D and T denote deuterium ($^2$H) and tritium ($^3$H), respectively.

Despite recent *ab initio* static studies of thermonuclear D-T fusion [3,4], the effect of a laser field on D-T fusion is not fully understood yet. Most existing theoretical models for describing this process are semiclassical and consider three stages [5]: (i) the evolution of a D-T classical trajectory towards the Coulomb barrier, (ii) the quantum tunneling process through the Coulomb barrier, and (iii) the calculation of the resultant fusion probability [6–8]. These models utilize the Wenzel-Kramers-Brillouin approximation for calculating the quantum tunneling probability, treating the D-T interaction potential as static for the duration of the fusion process. The dynamics of the laser field when calculating the tunneling process is neglected because the period of oscillation of the laser is considered much longer than the duration of the D-T interaction. In this regime, Refs. [7,8] report that the D-T fusion probabilities at low energies are enhanced by a laser-nucleus interaction, with the greatest enhancement owing to a strong laser field intensity ($\approx 10^{19}$ W cm$^{-2}$ and above). To our knowledge, quantum dynamical models for laser-assisted D-T fusion have not been explored yet. However, Refs. [9,10] discuss the effect of a laser field on both $\alpha$ and proton radioactivity using a fully quantum mechanical approach, showing that the decay process can be significantly affected by a laser field. The latter has been contested in Ref. [11]. In the present paper, we study the laser-assisted D-T fusion reaction using a quantum dynamical reaction method with the aim to verify the effects reported in Refs. [7,8]. We consider a single-channel, head-on D-T fusion reaction in the overall center-of-mass reference frame both with and without a laser field interaction. This interaction vastly increases the D-T fusion probability at subbarrier energies.

## II. MODEL

We consider the central collision of a deuterium projectile, of mass number $A_D$ and charge $Z_D e$, on a tritium target of mass number $A_T$ and charge $Z_T e$, so that $\mu = m_0 A_T A_D/(A_T + A_D)$ is the reduced mass of the D-T system and $m_0$ is the nucleon mass. This is because fusion probabilities for nonzero partial waves at subbarrier energies are negligible due to very high centrifugal barriers (e.g., the $p$-wave Coulomb barrier is 630% higher than the $s$-wave one). We first present the model in the absence of a laser field and subsequently include the laser-nucleus interaction. The initial radial relative motion of the D-T system is described in the overall center-of-mass reference frame by a Gaussian wave packet [12],

$$\Psi(r, t=0) = \mathcal{N}^{-1} \exp\left[-\frac{(r-r_0)^2}{2\sigma_0^2}\right] e^{-iK_0 r}, \qquad (1)$$

where $\mathcal{N} = \sqrt{\langle\Psi|\Psi\rangle}$ is the normalization constant; $r$ is the internuclear radius; $r_0$ is the initial, central position of the wave packet; $\sigma_0$ is the spatial dispersion; and $K_0$ is the average wave number, which depends on the average incident energy $E_0$, $r_0$, and $\sigma_0$ and is found by solving $E_0 = \langle\Psi|\hat{\mathcal{H}}_0|\Psi\rangle$ using the real part of the Hamiltonian in Eq. (5). The latter is because the initial wave packet is not free, but localized on the tail of the Coulomb potential. Since the initial state in Eq. (1) is not an eigenstate of the real part of $\hat{\mathcal{H}}_0$, the energy expectation value

TABLE I. Model variables for the simulations of the D-T nuclear fusion. Both the nuclear and absorption radius parameters, $R_0$ and $R_i$, should be multiplied by the dimensionless factor $A_D^{1/3} + A_T^{1/3}$.

| Variable | Value | Description |
|---|---|---|
| $A_D$ | 2 | Projectile mass number |
| $Z_D$ | 1 | Projectile proton number |
| $A_T$ | 3 | Target mass number |
| $Z_T$ | 1 | Target proton number |
| $\Delta r$ | 0.5 fm | Spatial step |
| $r_{\max}$ | 2000 fm | Maximum separation |
| $r_0$ | 1200 fm | Initial wave packet position |
| $\sigma_0$ | 300 fm | Wave packet spatial width |
| $\Delta t$ | 0.1 zs | Time step (1 zs $= 10^{-21}$ s) |
| $R_0$ | 0.95 fm | Nuclear radius parameter |
| $a_0$ | 0.55 fm | Nuclear diffuseness |
| $V_0$ | 40.4 MeV | Wood-Saxon potential depth |
| $R_i$ | 0.9 fm | Absorption radius parameter |
| $a_i$ | 0.3 fm | Absorption diffuseness |
| $W_0$ | 500 MeV | Absorption potential depth |

is complex and reads as

$$E_0 = \frac{\hbar^2 K_0^2}{2\mu} + \frac{\hbar^2}{4\mu\sigma_0^2} + \bar{V}(r_0, \sigma_0) + \frac{\hbar^2}{2\mu}\frac{1}{\sqrt{\pi}\left[1 + \mathrm{erf}\left(\frac{r_0}{\sigma_0}\right)\right]}\left[\frac{r_0}{\sigma_0^3} - i\frac{2K_0}{\sigma_0}\right]e^{-\left(\frac{r_0}{\sigma_0}\right)^2}. \quad (2)$$

To calculate $K_0$, the complex last term in Eq. (2) is neglected. For instance, using the parameters given in Table I and $E_0 = 100$ keV, its real and imaginary parts are respectively 7 and 6 orders of magnitude smaller than the second term in Eq. (2), which is approximately 0.1 keV.

We follow the time evolution of this wave packet in small timestep $\Delta t$ applying the unitary transformation [12],

$$\Psi(r, t + \Delta t) = U(t + \Delta t, t)\,\Psi(r, t), \quad (3)$$

where

$$U(t + \Delta t, t) \approx \frac{\left(1 - \frac{i\hat{\mathcal{H}}_0(r)\Delta t}{2\hbar}\right)}{\left(1 + \frac{i\hat{\mathcal{H}}_0(r)\Delta t}{2\hbar}\right)}, \quad (4)$$

and the Hamiltonian is

$$\hat{\mathcal{H}}_0(r) = -\frac{\hbar^2}{2\mu}\frac{\partial^2}{\partial r^2} + V(r) + iW(r). \quad (5)$$

The potential $V(r)$ in Eq. (5) stands for the total D-T interaction, which is the sum of a repulsive Coulomb potential and an attractive nuclear potential represented by a Woods-Saxon function with the depth $V_0$, the radius $R_0$, and the diffuseness parameter $a_0$ [13],

$$V(r) = \frac{Z_T Z_D e^2}{r} - \frac{V_0}{1 + \exp\left[\frac{r - R_0}{a_0}\right]}. \quad (6)$$

Figure 1 shows the total interaction potential (black solid line) and its Coulomb (blue dotted line) and nuclear (red dashed line) parts. The inset in Fig. 1 highlights the Coulomb barrier whose height of 190 keV and radius of 6.8 fm are very similar to those from the Sao Paulo double-folding potential model [14] that use $^2$H and $^3$H densities obtained from electron scattering experiments. The potential parameters are given in Table I.

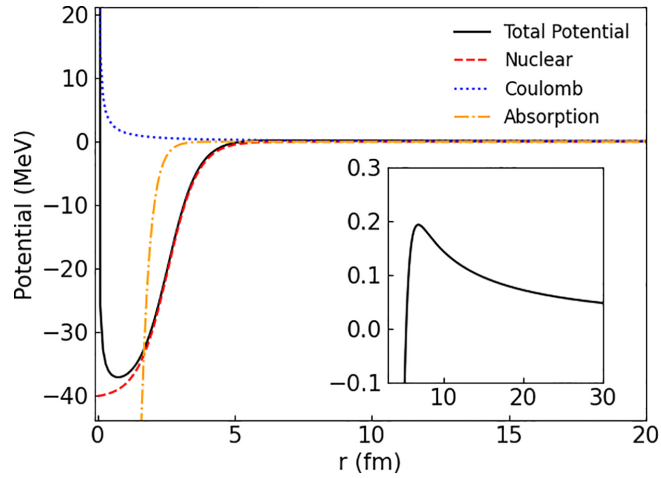


FIG. 1. Total interaction potential (black solid line) for a central D-T collision, which is the sum of an attractive nuclear potential (red dashed line) and a repulsive Coulomb potential (blue dotted line). A strong absorptive potential (orange dot-dashed line) to describe fusion is localized within the total potential pocket. The inset highlights the Coulomb barrier.

To account for fusion, a strong short-range imaginary potential [15] is used in Eq. (5),

$$W(r) = -\frac{W_0}{1 + \exp\left[\frac{r - R_i}{a_i}\right]}, \quad (7)$$

where the parameters are listed in Table I, and they guarantee complete absorption of the body of the wave packet trapped in the total potential pocket. This absorptive potential is shown in Fig. 1 by an orange dot-dashed line and is equivalent to an ingoing-wave boundary condition (IWBC) to study fusion [16]. The results weakly depend on the geometry of this potential, as long as it is well inside the Coulomb barrier and strong enough that the mean-free path of the reduced mass inside the barrier is much smaller than the dimensions of $W(r)$. This type of fusion model cannot describe resonant fusion and compound-elastic events, as the absorption is irreversible and only an average value of the fusion probability over the compound-nucleus resonance energies is determined [17]. To illustrate this point, Fig. 2 presents the theoretical fusion excitation function (black solid line) for D-T collisions, which is calculated by solving the time-independent Schrödinger equation (TISE) with the IWBC and the total interaction potential in Fig. 1. This static calculation is carried out using the modified Numerov method, as implemented in Ref. [18]. This TISE calculation is compared with the experimental fusion excitation function (symbols) that is dominated by the $J^\pi = 3/2^+$ resonance in $^5$He, which decays into $^4$He $+n$ [3,19,20]. Compound-elastic events are not recorded as fusion events in the experimental D-T fusion data. References [21,22] discuss

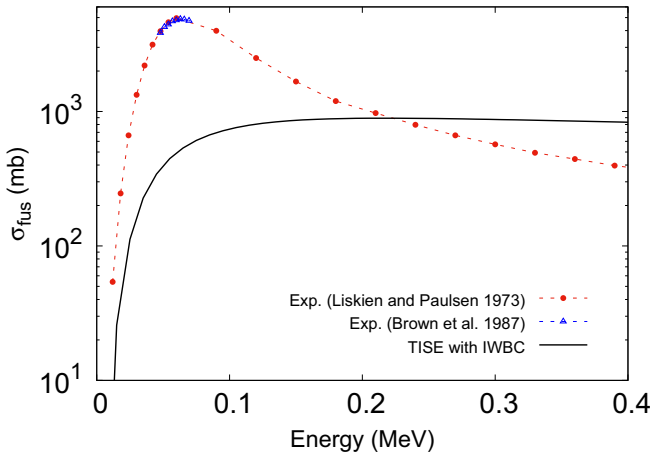


FIG. 2. Theoretical and experimental fusion excitation functions for low-energy D-T collisions. A model calculation based on either the time-independent Schrödinger equation (TISE) with the incoming-wave boundary condition (IWBC) or the present dynamical optical fusion model cannot address resonant fusion and compound-elastic events, which are relevant in the experimental fusion data [19,20].

static, optical fusion models based on a square-well nuclear potential for D-T collisions.

To calculate the fusion probability (transmission coefficient) with the present quantum dynamical model for a D-T collision, we determine the loss of norm of the initial wave packet due to the absorptive potential (i.e., $1 - \langle\Psi(t)|\Psi(t)\rangle$), as shown in Fig. 3. After a long propagation time $t_f$, this yields the stationary transmission coefficient,

$$\mathcal{T}(E_0) = 1 - \langle\Psi(t_f)|\Psi(t_f)\rangle, \tag{8}$$

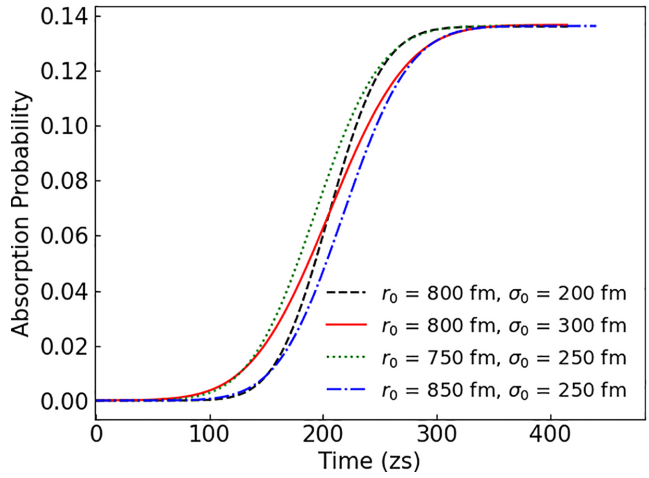


FIG. 3. Loss of norm of the incident wave packet (absorption probability) as a function of time in a central D-T collision with an initial average energy of $E_0 = 100$ keV. A stationary value, which is the transmission coefficient in Eq. (8), is established after a long propagation time, $t_f > 300$ zs. That value very weakly depends on both the initial location ($r_0$) and spatial width ($\sigma_0$) of the initial wave packet in Eq. (1).

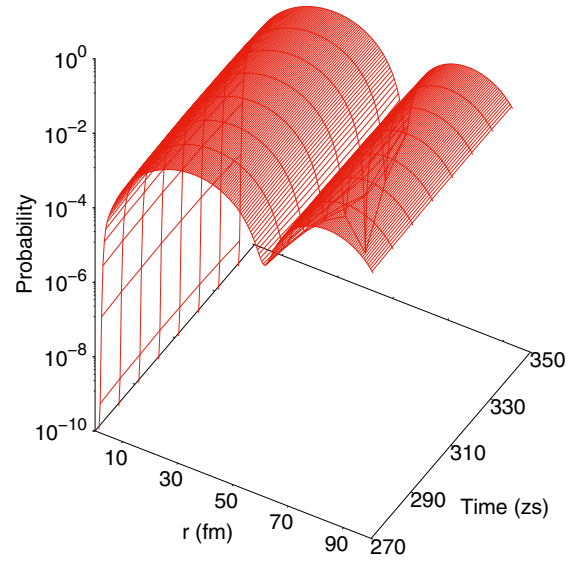


FIG. 4. Snapshots of the radial probability density of a wave packet describing a central D-T collision with an initial average energy of $E_0 = 100$ keV. For visualization, profiles of the probability density are shown every 10 zs, when the main body of the wave packet is around the Coulomb barrier region in Fig. 1.

for an initial average incident energy $E_0$. As seen in Fig. 3, this value very weakly depends on both the initial location ($r_0$) and spatial width ($\sigma_0$) of the initial wave packet in Eq. (1), provided they fulfill the criteria given below. A good accuracy of $\mathcal{T}(E_0)$ requires that the initial wave packet in Eq. (1) be (i) very broad in space, such that its energy variance, $\Delta E = \hbar^2/(4\mu\sigma_0^2)$, is very small compared with $E_0$, and (ii) spatially localized with $r_0$ very far from the distance of minimal approach of the Rutherford trajectory with $E_0$, i.e., $Z_D Z_T e^2/E_0$. These criteria are guaranteed with the parameters of the initial wave packet presented in Table I. For instance, the energy variance is $\Delta E \approx 0.1$ keV, which is much smaller than all the collision energies studied in the present work ($E_0 \geqslant 12$ keV). For $E_0 = 12$ keV, the classical turning point of the Rutherford trajectory is 120 fm, which is much smaller than $r_0 = 1200$ fm. The probability of the initial wave packet to be at radii smaller than 120 fm is negligible ($\approx 10^{-7}$). It decreases as $E_0$ increases, as the distance of minimal approach reduces with increasing $E_0$. Knowing $\mathcal{T}(E_0)$, the $s$-wave fusion cross section is $\sigma_{\rm fus}(E_0) = (\pi\hbar^2/2\mu E_0)\,\mathcal{T}(E_0)$.

Figure 4 presents profiles of the radial probability density for a wave packet with $E_0 = 100$ keV, when its main body scatters off the Coulomb barrier shown in Fig. 1. At short internuclear distances, where the absorption potential operates, there is no survival probability of the wave packet. Figure 5 shows the transmission coefficients calculated with Eq. (8) (blue dotted line) compared with those from TISE calculations (black dashed line). Their agreement is very good, confirming that Eq. (8) provides reliable fusion probabilities and, therefore, can be used to quantify the effects of laser-nucleus interaction on fusion.

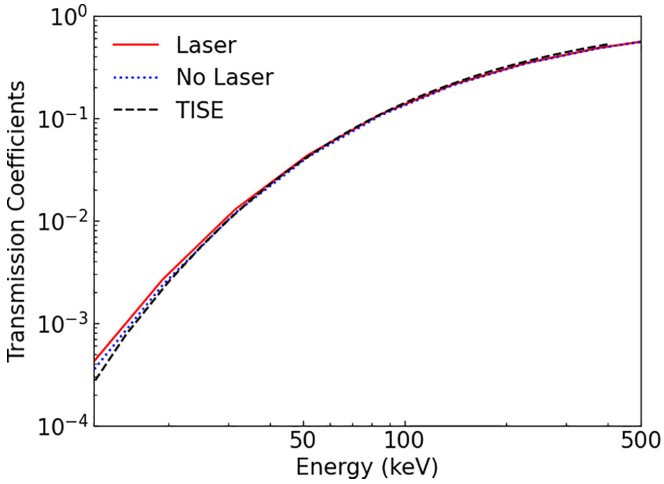


FIG. 5. Transmission coefficients for a central D-T fusion reaction both with and without a laser field (red solid and blue dotted lines, respectively), with varying initial average collision energies, compared with the TISE calculations (black dashed line). The laser parameters are $I = 10^{28}$ W cm$^{-2}$ and $\hbar\omega = 1$ eV. The Coulomb barrier height is 190 keV.

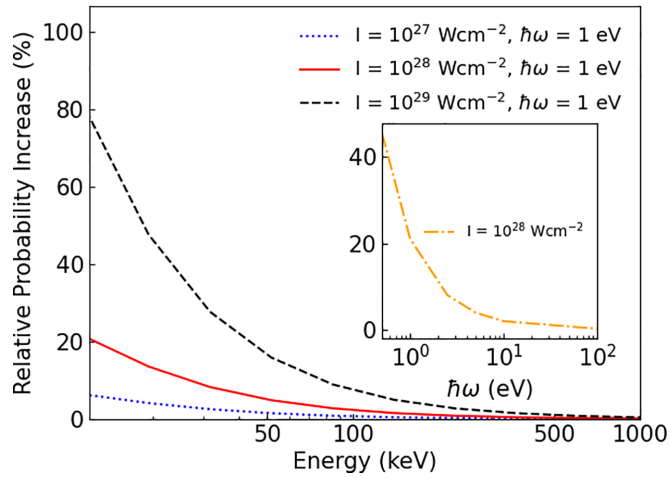


FIG. 6. The percentage enhancement of the subbarrier D-T fusion probabilities due to the laser-nucleus interaction for different values of intensity and photon energy of the laser field. The latter is shown in the inset for $E_0 = 12$ keV. The Coulomb barrier height is 190 keV.

### A. Laser-nucleus interaction

We follow Refs. [7,8] and redefine the system Hamiltonian by introducing a laser-nucleus interaction potential for a linearly polarized monochromatic laser field,

$$\hat{\mathcal{H}}(r,t) = \hat{\mathcal{H}}_0(r) + V_{\rm int}(r,t), \tag{9}$$

for $V_{\rm int}(r)$ given in the dipole approximation by

$$V_{\rm int}(r,t) = -\frac{e}{\mu} Z_{\rm eff} \vec{A}(t)\,\hat{p} + \frac{Z_{\rm eff}^2}{2\mu}\vec{A}^2(t), \tag{10}$$

where $\hat{p}$ is the radial linear momentum operator, $Z_{\rm eff}$ is the effective charge,

$$Z_{\rm eff} = \frac{Z_D A_T - Z_T A_D}{A_D + A_T}, \tag{11}$$

and $\vec{A}(t)$ is the vector potential of the laser field,

$$\vec{A}(t) = A_0 \cos(\omega t + \delta)\,\vec{e}_r, \tag{12}$$

for field strength $A_0 = \sqrt{2I/(\epsilon_0\, c\, \omega^2)}$, intensity $I$, frequency $\omega$, and phase factor $\delta$. In the calculations below, if not stated otherwise, we consider $\delta = 0$, $\hbar\omega = 1$ eV, and $I = 10^{28}$ W cm$^{-2}$. These parameters provide a large optimistic value of $A_0$ with currently achievable lasers [7], maximizing the effects of the laser-nucleus interaction on fusion. The strength of such effects declines when the angle between the laser's polarization axis and the internuclear radius increases towards $\pi/2$ [7,8].

Evolving the wave packet in this regime is exactly the same; however, we use Eq. (9) to describe our new Hamiltonian in Eq. (4). This change introduces a significant computational cost as we must update the Hamiltonian every time step $\Delta t$. For an average simulation of 500 zs, we multiply the total run time by a factor of 5000. Equation (8) can be applied to calculate the transmission coefficients affected by the laser field, as shown in Fig. 5 (red solid line).

## III. RESULTS AND DISCUSSION

Figure 5 shows that the laser field enhances the transmission coefficients for D-T fusion (red solid line) relative to the scenario without a laser (blue dotted line). This is more visible in Fig. 6 (red solid line), which shows the transmission coefficient's enhancement induced by the laser as a function of the average incident energy. Clearly, a significant enhancement of the deep subbarrier D-T fusion probabilities due to the laser-nucleus interaction occurs. In Fig. 6, it is observed that the percentage enhancement increases with increasing intensity of the laser, while an increased value of the photon energy reduces the enhancement of the fusion probability (inset). The present results qualitatively agree with those in Refs. [7,8], but our percentage enhancement of fusion is (i) an order of magnitude smaller than the value found in Ref. [7] using an analytical method within the Kramers-Henneberger (KH) framework [23] in the high-frequency limit ($\hbar\omega \approx 1$ keV) and (ii) various orders of magnitude smaller than the enhancement reported in Ref. [8] using a semiclassical model in both the high- and low-frequency ($\hbar\omega \approx 1$ eV) limits. The physical reason for the fusion enhancement is the *quiver* motion of the D-T system's effective charge [8–10], which is caused by the first term in Eq. (10). The maximal amplitude of this radial *Zitterbewegung*, $\alpha_0 = eZ_{\rm eff}A_0/\mu\omega$, increases with increased intensity and decreased frequency of the laser field. In the KH representation of the wave packet [23], the effect of the laser field on the D-T fusion dynamics is fully transferred into the argument of both the absorptive potential and the total interaction potential shown in Fig 1, e.g., $V(r - \alpha_0 \sin\omega t)$. The potential in the inset of Fig. 1 would be radially shaking, which allows the potential pocket to capture more probability from the incident wave packet.

## IV. SUMMARY

We have presented a quantum dynamical approach to low-energy D-T fusion. It was successfully tested against the solution of the time-independent Schrödinger equation. The present fusion model describes the average trend of the D-T fusion excitation function. This average fusion baseline can be significantly enhanced by effects of a laser-nucleus interaction at deep subbarrier energies using very intense lasers with low frequency. Coupled-channels fusion calculations for laser-assisted low-energy heavy-ion collisions are in progress and will be reported elsewhere.

## ACKNOWLEDGMENTS

This work was supported by the United Kingdom Science and Technology Facilities Council (STFC) under Grant No. ST/W507842/1 and by the Leverhulme Trust (U.K.) under Grant No. RPG-2019-325.

[1] ITER organization, home page (2024), https://iter.org.
[2] Lawrence Livermore National Laboratory, National Ignition Facility and Photon Science, home page (2024), https://lasers.llnl.gov.
[3] G. Hupin, S. Quaglioni, and P. Návratil, *Ab-initio* predictions for polarized deuterium-tritium thermonuclear fusion, Nat. Commun. **10**, 351 (2019).
[4] P. Návratil and S. Quaglioni, *Ab initio* many-body calculations of the $^3$H$(d,n)^4$He and $^3$He$(d,p)^4$He fusion reactions, Phys. Rev. Lett. **108**, 042503 (2012).
[5] J. J. Bekx, M. L. Lindsey, S. H. Glenzer, and K.-G. Schlesinger, Applicability of semiclassical methods for modeling laser-enhanced fusion rates in a realistic setting, Phys. Rev. C **105**, 054001 (2022).
[6] F. Queisser and R. Schützhold, Dynamically assisted nuclear fusion, Phys. Rev. C **100**, 041601(R) (2019).
[7] W. Lv, H. Duan, and J. Liu, Enhanced deuterium-tritium fusion cross sections in the presence of strong electromagnetic fields, Phys. Rev. C **100**, 064610 (2019).
[8] S. Liu, H. Duan, D. Ye, and J. Liu, Deuterium-tritium fusion process in strong laser fields: Semiclassical simulation, Phys. Rev. C **104**, 044614 (2021).
[9] Ş Mişicu and M. Rizea, $\alpha$-decay in ultra-intense laser fields, J. Phys. G: Nucl. Part. Phys. **40**, 095101 (2013).
[10] Ş Mişicu and M. Rizea, Laser-assisted proton radioactivity of spherical and deformed nuclei, J. Phys. G: Nucl. Part. Phys. **46**, 115106 (2019).
[11] A. Pálffy and S. V. Popruzhenko, Can extreme electromagnetic fields accelerate the $\alpha$ decay of nuclei? Phys. Rev. Lett. **124**, 212505 (2020).
[12] D. Tannor, *Introduction to Quantum Mechanics: A Time Dependent Perspective* (University Science Books, Sausalito, 2007).
[13] A. B. Balantekin and N. Takigawa, Quantum tunneling in nuclear fusion, Rev. Mod. Phys. **70**, 77 (1998).
[14] L. C. Chamon, B. V. Carlson, and L. R. Gasques, São Paulo potential version 2 (SPP2) and Brazilian nuclear potential (BNP), Comput. Phys. Commun. **267**, 108061 (2021).
[15] T. Vockerodt and A. Diaz-Torres, Describing heavy-ion fusion with quantum coupled-channels wave-packet dynamics, Phys. Rev. C **100**, 034606 (2019).
[16] S. Landowne and S. C. Pieper, Coupled-channels fusion calculations for $^{58}$Ni + $^{58}$Ni, Phys. Rev. C **29**, 1352 (1984).
[17] H. Feshbach, C. E. Porter, and V. F. Weisskopf, Model for nuclear reactions with neutrons, Phys. Rev. **96**, 448 (1954).
[18] K. Hagino, N. Rowley, and A. T. Kruppa, A program for coupled-channel calculations with all order couplings for heavy-ion fusion reactions, Comput. Phys. Commun. **123**, 143 (1999).
[19] H. Liskien and A. Paulsen, Neutron production cross sections and energies for the reactions T$(p,n)^3$He, D$(d,n)^3$He, and T$(d,n)^4$He, At. Data Nucl. Data Tables **11**, 569 (1973).
[20] R. E. Brown, N. Jarmie, and G. M. Hale, Fusion-energy reaction $^3$H$(d,\alpha)n$ at low energies, Phys. Rev. C **35**, 1999 (1987).
[21] X. Z. Li, J. Tian, M. Y. Mei, and C. X. Li, Sub-barrier fusion and selective resonant tunneling, Phys. Rev. C **61**, 024610 (2000).
[22] B. Wu, H. Duan, and J. Liu, Resonant tunneling of deuteron-tritium fusion in strong high-frequency electromagnetic fields, Phys. Rev. C **105**, 064615 (2022).
[23] W. C. Henneberger, Perturbation method for atoms in intense light beams, Phys. Rev. Lett. **21**, 838 (1968).